Princeton Plasma Physics Laboratory

PPPL- 4882

PPPL- 4882

A Variational Multi-Symplectic PIC Algorithm with Smoothing Functions for the Vlasov-Maxwell System

J. Xiao, J. Liu, H. Qin and Z. Yu

May, 2013

PPPL PRINCETON PLASMA PHYSICS LABORATORY

Prepared for the U.S. Department of Energy under Contract DE-AC02-09CH11466.

Princeton Plasma Physics Laboratory
Report Disclaimers

Full Legal Disclaimer

Trademark Disclaimer

PPPL Report Availability

Princeton Plasma Physics Laboratory:

http://www.pppl.gov/techreports.cfm

Office of Scientific and Technical Information (OSTI):

http://www.osti.gov/bridge

Related Links:

U.S. Department of Energy

Office of Scientific and Technical Information

Fusion Links

A Variational Multi-Symplectic PIC Algorithm with Smoothing Functions for the Vlasov-Maxwell System*

Jianyuan Xiao,[1] Jian Liu,[1,†] Hong Qin,[1,2] and Zhi Yu[3]

[1]*Department of Modern Physics and Collaborative Innovation Center for Advanced Fusion Energy and Plasma Sciences, University of Science and Technology of China, Hefei, Anhui 230026, China*

[2]*Plasma Physics Laboratory, Princeton University, Princeton, New Jersey 08543, USA*

[3]*Theory and Simulation Division, Institute of Plasma Physics, Chinese Academy of Sciences, Hefei, Anhui 230031, China*

Abstract

Smoothing functions are commonly used to reduce numerical noises arising from coarse sampling of particles in particle-in-cell (PIC) plasma simulations. When applying smoothing functions to symplectic algorithms, the conservation of symplectic structure should be guaranteed to preserve good conservation properties. In this paper, we show how to construct a variational multi-symplectic PIC algorithm with smoothing functions for the Vlasov-Maxwell system. The conservation of the multi-symplectic structure and the reduction of numerical noises make this algorithm specifically suitable for simulating long-term dynamics of plasmas, such as those in the steady-state operation or long-pulse discharge of a super-conducting tokamak. The algorithm has been implemented in a 6D large scale PIC code. Numerical examples are given to demonstrate the good conservation properties of the multi-symplectic algorithm and the reduction of the noise due to the application of smoothing function.

* This research is supported by ITER-China Program (2010GB107001, 2013GB111000), the Fundamental Research Funds for the Central Universities (WK2030020022), China Postdoctoral Science Foundation (2013M530296), and the National Natural Science Foundation of China (NSFC-11075162).

† jliuphy@ustc.edu.cn

I. INTRODUCTION

Modern large-scale simulations in plasma physics require algorithms with long-term numerical stability and high computation efficiency. When facing multi-time-scale problems, such as RF wave heating and current drive in tokamaks, the coherent accumulation of numerical errors turns out to be the most challenging problem. Standard algorithms can bound numerical errors from each time-step by small values, but they do not guarantee that numerical errors from different time-steps cancel out with each other. In general, the total numerical error increases through accumulation over many time-steps. This problem can be resolved by using symplectic integrators which bound the total numerical error of energy and momentum, and conserve phase space volume of a physical system [1]. The basic idea of symplectic integrator is to construct integrators which exactly conserve a discrete symplectic two-form, the so-called symplectic structure. Different approaches to constructing symplectic integrators have been developed [2–9]. A standard method [2–4] is to investigate the generating functions of dynamic systems. Because this method requires canonical Hamiltonian structure, its application is limited. It cannot be applied to non-canonical Hamilton systems, such as the gyrocenter systems, and particle-field systems conveniently. Marsden, et al., proposed another method to obtain symplectic integrators based on the discretization of the Lagrangian of the system [10]. Through discrete variational principle, this method can be applied to the gyrocenter systems [11, 12] and the evolution of electromagnetic field, an infinite dimensional system described by partial differential equations (PDE). Based on a similar idea, variational multisymplectic integrators using discrete exterior calculus (DEC) technique have also recently been developed [13, 14].

In the particle-in-cell (PIC) method, fields and particles are sampled in different ways. Fields are sampled on Eulerian grids in 3D configuration space, while particles are sampled on Lagrangian grids in 6D phase space. The PIC method greatly enhances computation efficiency while avoiding the singularity problem [15]. Due to the limit of computation capacity, it is unpractical to track down the trajectories of all real particles. A sampling point, namely a marker or super-particle, is hence used to denote a number of real particles to relieve the computation burden. On the other hand, the coarse sampling leads to a large background noise, which is the major drawback of full-f PIC methods. In addition to increasing the number of markers, various techniques have been developed to suppress

the numerical noises, such as the δf method and the application of smoothing functions. A smoothing function, also called as a shape function [16], is a local distribution function carried by each marker to give the marker a smoother shape (compared with the sharp δ-function shape). However, the application of smoothing functions in symplectic integrator is not as simple as in standard algorithms, because the application of smoothing functions may break the symplectic structure.

As a generalization of original variational symplectic algorithm, a variational multisymplectic integrator with a smoothing function S for the Vlasov-Maxwell system is necessary for its application to PIC plasma simulation. In this paper, we show how to develop such a symplectic algorithm based on the Lagrangian of the system. We follow Marsden's procedure [10, 17] to construct the variational symplectic integrator and give an explicit particle pusher which is less resources consuming. The challenge is how to preserve the symplectic structure of entire self-consistent particle-field system while allowing different smoothing functions for particle sampling. A selected smoothing function, which reflects the form of particles' local distribution at each sampling point, is substituted into the Lagrangian at the very beginning. After taking variation of the discretized Lagrangian, we obtain a discrete symplectic integrator with smoothing function for the entire Maxwell-Vlasov system. This algorithm is realized in a PIC code, where the good conservation properties of the algorithm are numerically verified. We also compare cases with different smoothing functions to demonstrate the effectiveness of noise suppression.

The paper is organized as follows. In section II, the detailed procedure of constructing a variational multi-symplectic PIC algorithm with smoothing function is introduced. In Section III, we describe the implementation of this algorithm in a PIC code. Three numerical examples are given to demonstrate the good conservation properties of this symplectic algorithm and the reduction of numerical noises due to the application of smoothing function. Finally we briefly summarize and discuss future plans in Section IV.

II. CONSTRUCTION OF THE VARIATIONAL SYMPLECTIC PIC ALGORITHM WITH SMOOTHING FUNCTION FOR THE MAXWELL-VLASOV SYSTEM

In this section, we construct a generalized variational symplectic PIC algorithm with smoothing function for the Vlasov-Maxwell system. The starting point is the Lagrangian

of a Vlasov-Maxwell system and the corresponding variational principle. In the context of classical dynamics, the Lagrangian density for a collection of N non-relativistic charged particles together with the electromagnetic field is [18, 19]

$$\begin{aligned}\mathcal{L} =& \frac{\epsilon_0}{2}\left[-\dot{\mathbf{A}}\left(\mathbf{x}\right)-\nabla\phi\left(\mathbf{x}\right)\right]^2-\frac{1}{2\mu_0}\left[\nabla\times\mathbf{A}\left(\mathbf{x}\right)\right]^2 \\ &+\sum_{s=1}^{N}\delta\left(\mathbf{x}-\mathbf{x}_s\right)\left[\frac{1}{2}m_s\dot{\mathbf{x}}_s^2+\mathrm{q}_s\mathbf{A}\left(\mathbf{x}\right)\cdot\dot{\mathbf{x}}_s-\mathrm{q}_s\phi\left(\mathbf{x}\right)\right], \end{aligned} \tag{1}$$

where m_s, q_s, and $\mathbf{x}_s$ denote the mass, electric charge, and position of the s-th particle respectively, ε_0 is the permittivity of free space, μ_0 is the permeability of free space, and $\mathbf{A}$ and ϕ are vector potential and scalar potential for the electromagnetic field. The corresponding Lagrangian L is the integral of $\mathcal{L}$ over configuration space

$$L=\iiint_{\Omega}\mathcal{L}\mathrm{d}^3\mathbf{x}\ , \tag{2}$$

and the action $\mathcal{A}$ is the integral of L over time

$$\mathcal{A}=\int_{t_0}^{t_1}L\mathrm{d}t\ . \tag{3}$$

According to Hamilton's principle, the evolution of the Vlasov-Maxwell system is determined by the variational equations with respect to independent variables $\mathbf{A},\phi,\mathbf{x}_s$, that is,

$$\frac{\delta\mathcal{A}}{\delta\mathbf{A}}=0\ , \tag{4}$$

$$\frac{\delta\mathcal{A}}{\delta\phi}=0\ , \tag{5}$$

$$\frac{\delta\mathcal{A}}{\delta\mathbf{x}_s}=0\ . \tag{6}$$

Equation (4) gives Ampère's law

$$\nabla\times\mathbf{B}=\mu_0\sum_s q_s\delta\left(\mathbf{x}-\mathbf{x}_s\right)\dot{\mathbf{x}}_s+\mu_0\epsilon_0\frac{\partial\mathbf{E}}{\partial t}\ . \tag{7}$$

Equation (5) gives Gauss's law

$$\nabla\cdot\mathbf{E}=\epsilon_0\sum_s q_s\delta\left(\mathbf{x}-\mathbf{x}_s\right)\ , \tag{8}$$

and Eq. (6) gives the motion equation of charged particles

$$m_s\ddot{\mathbf{x}}_s=q_s\left(\mathbf{v}_s\times\mathbf{B}+\mathbf{E}\right). \tag{9}$$

Gauss's law for magnetism

$$\nabla \cdot \mathbf{B} = 0 \tag{10}$$

and Faraday's law of induction

$$\nabla \times \mathbf{E} = -\frac{\partial \mathbf{B}}{\partial t} \tag{11}$$

follow directly from the definition of $\mathbf{E}$ and $\mathbf{B}$,

$$\mathbf{B} = \nabla \times \mathbf{A} \ , \tag{12}$$

$$\mathbf{E} = -\frac{\partial \mathbf{A}}{\partial t} - \nabla\phi \ . \tag{13}$$

Therefore Eqs. (4) to (6) are equivalent to the Vlasov-Maxwell system. Our task is to discretize this set of equations into symplectic difference equations suitable for PIC simulations.

In PIC method, field quantities are sampled on fixed grids in configuration space. A rectangular region in 3D configuration space is discretized to rectangular grids (i, j, k) with the same grid spacing Δl, where i, j, and k are integer indices for three directions of the chosen Cartesian coordinate frame. The integers N_x, N_y, and N_z are grid numbers in three directions with $1 \leq i \leq N_x, 1 \leq j \leq N_y, 1 \leq k \leq N_z$. Potentials on grids are denoted as $\mathbf{A}_{i,j,k} = \mathbf{A}(\mathbf{x}_{i,j,k})$ and $\phi_{i,j,k} = \phi(\mathbf{x}_{i,j,k})$. In Eq. (1) potentials in the positions of particles are required, while almost all particles do not locate on grids exactly. Off-grid values of potentials can be calculated by interpolation techniques as

$$\mathbf{A}\left(\mathbf{x}\right) = \sum_{i,j,k} \mathbf{A}_{i,j,k} W(\mathbf{x} - \mathbf{x}_{i,j,k}) \ , \tag{14}$$

$$\phi\left(\mathbf{x}\right) = \sum_{i,j,k} \phi_{i,j,k} W(\mathbf{x} - \mathbf{x}_{i,j,k}) \ , \tag{15}$$

where W denotes the interpolation function. Though it seems that summations in Eqs. (14) and (15) are taken over all the spatial grids, practical sum operation only involves the grids adjacent to the position $\mathbf{x}$, because the value of W is not zero only in a small region around $\mathbf{x}$. The accuracy of interpolation determines the smoothness of the electromagnetic fields in PIC simulations. Given an interpolation function W, the Lagrangian L can be expressed as a function of field values on grids according to Eqs. (1) and (2).

On the other hand, particles are sampled in PIC method on Lagrangian grids which are carried by charged particles. However, due to the constraint on computing power, it's impossible to trace the trajectory of every particle. To reduce the computation burden, a

sampling point is used to present a group of particles in practical PIC simulations. Thus the third term on the right-hand-side (RHS) of Eq. (1) ought to be modified accordingly. The summation over charged particles should be replaced by a summation over markers, and distributions of particles in configuration space $\delta\left(\mathbf{x}_s-\mathbf{x}\right)$ should be replaced by distributions carried by markers $S(\mathbf{x},\mathbf{x}_s)$. The smoothing function $S(\mathbf{x},\mathbf{x}_s)$ represents the shape of particle distribution in configuration space carried by the s-th marker [16]. Smoothing functions have to bear properties such as symmetry and normalization, and thus can be further written as $S(\mathbf{x}-\mathbf{x}_s)$. The simplest smoothing function is still the delta function $\delta\left(\mathbf{x}_s-\mathbf{x}\right)$, which indicates that all the particles represented by the s-th marker locate in a same position $\mathbf{x}_s$. Obviously, such a choice brings large numerical noises. A better smoothing function should span a finite volume, characterized by a length parameter a, in configuration space. In the first paper on SPH (Smoothed-particle hydrodynamics) [20], Lucy used a bell-shaped smoothing function

$$S(R;a)=\alpha_d\begin{cases}(1+3R)(1-R)^3 & R\leq 1\ ,\\ 0 & R>1\ ,\end{cases} \tag{16}$$

where $R=|(\mathbf{x}-\mathbf{x}_s)/a|$ is the relative distance and α_d is the normalization coefficient for the number of dimensions d. Larger parameter a usually leads to lower numerical noises but requires larger computing power.

After dealing with the sampling problem of fields and particles, we have to discretize the Lagrangian containing interpolation function and smoothing function. To introduce the discretization procedure, we separate the Lagrangian into three parts,

$$L=L_f+L_I+L_p\ , \tag{17}$$

where the Lagrangian for fields is

$$L_f=\iiint_\Omega\frac{1}{2}\left(\epsilon_0\left(\dot{\mathbf{A}}\left(\mathbf{x}\right)+\nabla\phi\left(\mathbf{x}\right)\right)^2-\frac{1}{\mu_0}\left(\nabla\times\mathbf{A}\left(\mathbf{x}\right)\right)^2\right)\mathrm{d}\mathbf{x}\ , \tag{18}$$

the Lagrangian for particles is

$$L_p=\iiint_\Omega\sum_s\frac{1}{2}S(\mathbf{x}_s-\mathbf{x},a)m_s\dot{\mathbf{x}}_s^2\mathrm{d}\mathbf{x}=\frac{1}{2}m_s\dot{\mathbf{x}}_s^2\ , \tag{19}$$

and the Lagrangian for interaction between particles and fields is

$$L_I=\iiint_\Omega\sum_s q_sS(\mathbf{x}_s-\mathbf{x},a)\left(\mathbf{A}\left(\mathbf{x}\right)\cdot\dot{\mathbf{x}}_s-\phi\left(\mathbf{x}\right)\right)\mathrm{d}\mathbf{x}\ . \tag{20}$$

The second equality sign in Eq. (19) holds because of the normalization of smoothing function. Therefore, the smoothing function does not appear in L_p any more. Note that m_s here denotes the mass of the s-th marker, which indicates its weight implicitly.

When substituting interpolated potential functions given by Eqs. (14) and (15) into the Lagrangian of Eqs. (18) to (20), the dependence of L_f, L_I, and L_p on $\mathbf{A}_{i,j,k}$, $\phi_{i,j,k}$, $\dot{\mathbf{A}}_{i,j,k}$, $\mathbf{x}_s$, and $\dot{\mathbf{x}}_s$ are

$$L_f = L_f\left(\dot{\mathbf{A}}_{i,j,k}, \mathbf{A}_{i,j,k}, \phi_{i,j,k}\right) \ , \tag{21}$$

$$L_I = L_I\left(\mathbf{A}_{i,j,k}, \phi_{i,j,k}, \dot{\mathbf{x}}_s, \mathbf{x}_s\right) \ , \tag{22}$$

$$L_p = L_p\left(\dot{\mathbf{x}}_s\right) \ . \tag{23}$$

The time variable can also be discretized uniformly to N_t time steps with time interval Δt. We use the forth subscript l to denote the time coordinate for discretized variables. Then the action of fields

$$\mathcal{A}_f = \int_0^{N_t \Delta t} L_f \mathrm{d}t \tag{24}$$

can be discretized as

$$\tilde{\mathcal{A}}_f = \sum_{l=0}^{N_t-1} \tilde{L}_f(l, l+1)\Delta t \ , \tag{25}$$

where

$$\tilde{L}_f\left(l, l+1\right) = L_f\left(\dot{\mathbf{A}}_{i,j,k,l+1/2}, \mathbf{A}_{i,j,k,l+1/2}, \phi_{i,j,k,l+1/2}\right) \tag{26}$$

is the discretized Lagrangian of field on time interval $[l\Delta t, (l+1)\Delta t]$. The field variables on half time-steps take the form of

$$\mathbf{A}_{i,j,k,l+1/2} = \frac{\mathbf{A}_{i,j,k,l} + \mathbf{A}_{i,j,k,l+1}}{2} \ , \tag{27}$$

$$\phi_{i,j,k,l+1/2} = \frac{\phi_{i,j,k,l} + \phi_{i,j,k,l+1}}{2} \ . \tag{28}$$

The time derivative $\dot{\mathbf{A}}_{i,j,k,l+1/2}$ is discretized as

$$\dot{\mathbf{A}}_{i,j,k,l+1/2} = \frac{\mathbf{A}_{i,j,k,l+1} - \mathbf{A}_{i,j,k,l}}{\Delta t} \ . \tag{29}$$

Similarly, the action of particles

$$\mathcal{A}_p = \int_0^{N_t \Delta t} L_p \mathrm{d}t \tag{30}$$

can be discretized as

$$\tilde{\mathcal{A}}_p = \sum_{l=0}^{N_t-1} \tilde{L}_p(l, l+1)\Delta t \ , \tag{31}$$

$$\tilde{L}_p(l, l+1) = L_p\left(\dot{\mathbf{x}}_{s,l+1/2}\right) \ . \tag{32}$$

The time derivative $\dot{\mathbf{x}}_{s,l+1/2}$ is discretized as

$$\dot{\mathbf{x}}_{s,l+1/2} = \frac{\mathbf{x}_{s,l+1} - \mathbf{x}_{s,l}}{\Delta t} \ . \tag{33}$$

If we repeat midpoint scheme when discretizing the action of interaction $\mathcal{A}_i$, the particle pusher would be totally implicit. To develop a more efficient pusher, we use a different method. The action of interaction

$$\mathcal{A}_I = \int_0^{N_t\Delta t} L_I \mathrm{d}t \tag{34}$$

is discretized as

$$\tilde{\mathcal{A}}_I = \sum_{l=0}^{N_t-1} \tilde{L}_I(l, l+1)\Delta t \ , \tag{35}$$

$$\tilde{L}_i(l, l+1) = L_I\left(\mathbf{A}_{i,j,k,l}, \phi_{i,j,k,l}, \dot{\mathbf{x}}_{s,l+1/2}, \mathbf{x}_{s,l}\right) . \tag{36}$$

The total discretized action is the summation of three parts,

$$\tilde{\mathcal{A}} = \tilde{\mathcal{A}}_f + \tilde{\mathcal{A}}_p + \tilde{\mathcal{A}}_I \ . \tag{37}$$

We now applies the discrete variational principle to derive a multi-symplectic integrator. Corresponding to Eqs. (4) to (6), the discretized Hamilton's principle are expressed as

$$\frac{\partial \tilde{\mathcal{A}}}{\partial \mathbf{A}_{i,j,k,l}} = 0 \ , \tag{38}$$

$$\frac{\partial \tilde{\mathcal{A}}}{\partial \phi_{i,j,k,l}} = 0 \ , \tag{39}$$

$$\frac{\partial \tilde{\mathcal{A}}}{\partial \mathbf{x}_{s,l}} = 0 \tag{40}$$

for each i, j, k, s, and l. Because the initial and final states are fixed, variations at time-step 0 and N_t should be zero, that is,

$$(\delta\mathbf{A}_{i,j,k,0}, \delta\phi_{i,j,k,0}, \delta\mathbf{x}_{s,0}) = (\delta\mathbf{A}_{i,j,k,N_t}, \delta\phi_{i,j,k,N_t}, \delta\mathbf{x}_{s,N_t}) = (0, 0, 0) \ . \tag{41}$$

Equations (38) and (39) provide the discretized Maxwell solver, and Eq. (40) provides the discretized particle pusher.

For the action of fields $\tilde{\mathcal{A}}_f$, which does not depend on $\mathbf{x}_{s,l}$, we have

$$\frac{\tilde{\mathcal{A}}_f}{\partial \mathbf{A}_{i,j,k,l}} = \Delta t \left(\frac{\partial \tilde{L}_f(l-1,l)}{\partial \mathbf{A}_{i,j,k,l}} + \frac{\partial \tilde{L}_f(l,l+1)}{\partial \mathbf{A}_{i,j,k,l}} \right) , \tag{42}$$

$$\frac{\tilde{\mathcal{A}}_f}{\partial \phi_{i,j,k,l}} = \Delta t \left(\frac{\partial \tilde{L}_f(l-1,l)}{\partial \phi_{i,j,k,l}} + \frac{\partial \tilde{L}_f(l,l+1)}{\partial \phi_{i,j,k,l}} \right) . \tag{43}$$

Substituting Eqs. (14) and (15) into Eq. (26), we have

$$\begin{aligned} \tilde{L}_f\left(l,l+1\right) =& \frac{\epsilon_0}{2} \iiint_\Omega \mathrm{d}^3\mathbf{x} \left(\sum_{i,j,k} \dot{\mathbf{A}}_{i,j,k,l+1/2} W_{i,j,k}\left(\mathbf{x}\right) + \sum_{i,j,k} \phi_{i,j,k,l+1/2} \nabla W_{i,j,k}\left(\mathbf{x}\right) \right)^2 \\ & - \frac{1}{2\mu_0} \iiint_\Omega \mathrm{d}^3\mathbf{x} \left(\sum_{i,j,k} \nabla \times \mathbf{A}_{i,j,k,l+1/2} W_{i,j,k}\left(\mathbf{x}\right) \right)^2 , \end{aligned} \tag{44}$$

where $W_{i,j,k}\left(\mathbf{x}\right) = W\left(\mathbf{x} - \mathbf{x}_{i,j,k}\right)$ is the interpolation function. From Eqs. (27) to (29), it is clear that $\tilde{L}_f\left(l,l+1\right)$ is a quadratic form of $\mathbf{A}_{i,j,k,l}$, $\mathbf{A}_{i,j,k,l+1}$, $\phi_{i,j,k,l}$ and $\phi_{i,j,k,l+1}$, which asserts that Eqs. (42) and (43) are both linear equations. It's also obvious that only $\tilde{L}_f(l,l+1)$ and $\tilde{L}_f(l-1,l)$ contain values on the l-th time-step, such as $\mathbf{A}_{i,j,k,l}$ and $\phi_{i,j,k,1}$.

For the variation of the action of interaction $\tilde{\mathcal{A}}_I$ with respect to vector potential, we have

$$\frac{\partial \tilde{\mathcal{A}}_i}{\partial \mathbf{A}_{i,j,k,l}} = \Delta t \sum_s \iiint q_s S(\mathbf{x} - \mathbf{x}_{s,l}; a) W_{i,j,k}(\mathbf{x}) \dot{\mathbf{x}}_{s,l+1/2} \mathrm{d}\mathbf{x} = \Delta t \mathbf{J}_{i,j,k,l} , \tag{45}$$

which gives the current density on grids. The variation with respect to the scalar potential gives the electric charge density on grids,

$$\frac{\partial \tilde{\mathcal{A}}_i}{\partial \phi_{i,j,k,l}} = -\Delta t \sum_s \iiint q_s S(\mathbf{x} - \mathbf{x}_{s,l}; a) W_{i,j,k}(\mathbf{x}) \mathrm{d}\mathbf{x} = -\Delta t \rho_{i,j,k,l} . \tag{46}$$

Noting that the action of particles $\tilde{\mathcal{A}}_p$ is independent of field variables, we can write down the variational equations for the total action as

$$\frac{\partial \tilde{\mathcal{A}}}{\partial \mathbf{A}_{i,j,k,l}} = \frac{\partial (\tilde{\mathcal{A}}_f + \tilde{\mathcal{A}}_i)}{\partial \mathbf{A}_{i,j,k,l}} = 0 , \tag{47}$$

and

$$\frac{\partial \tilde{\mathcal{A}}}{\partial \phi_{i,j,k,l}} = \frac{\partial (\tilde{\mathcal{A}}_f + \tilde{\mathcal{A}}_i)}{\partial \phi_{i,j,k,l}} = 0 . \tag{48}$$

It can be proved that Eqs. (47) and (48) are also linear equations of $\mathbf{A}_{i,j,k,l+1}$ and $\phi_{i,j,k,l+1}$. Thus according to Eqs. (47) and (48), we can solve for field variables at the $(l+1)$-th

time-step $\mathbf{A}_{i,j,k,l+1}$ and $\phi_{i,j,k,l+1}$ from field variables at previous time-steps $\mathbf{A}_{i,j,k,l-1}$, $\mathbf{A}_{i,j,k,l}$, $\phi_{i,j,k,l-1}$, $\phi_{i,j,k,l}$ and $\mathbf{J}_{i,j,k,l}$, $\rho_{i,j,k,l}$ using conjugate gradient method [21].

Because the action of fields $\tilde{\mathcal{A}}$ doesn't depend on $\mathbf{x}_s$, Eq. (40) can be written as

$$\frac{1}{\Delta t}\frac{\partial \tilde{\mathcal{A}}}{\partial \mathbf{x}_{s,l}} = \frac{\partial}{\partial \mathbf{x}_{s,l}}\left[\tilde{L}_i\left(l-1,l\right)+\tilde{L}_i\left(l,l+1\right)+\tilde{L}_p\left(l,l-1\right)+\tilde{L}_p\left(l,l+1\right)\right]=0\ , \tag{49}$$

where

$$-\frac{1}{m_s}\frac{\partial}{\partial \mathbf{x}_{s,l}}\left[\tilde{L}_p\left(l-1,l\right)+\tilde{L}_p\left(l,l+1\right)\right]=\frac{1}{\Delta t^2}\left(\mathbf{x}_{s,l-1}-2\mathbf{x}_{s,l}+\mathbf{x}_{s,l+1}\right) \tag{50}$$

can be regarded as the discrete acceleration of the s-th marker at the l-th time-step. The Lagrangian of interaction is expressed explicitly as

$$\tilde{L}_i\left(l,l+1\right)= \iiint_{\Omega}\sum_{i,j,k,s} q_s S(\mathbf{x}_{s,l}-\mathbf{x},a)\left(\mathbf{A}_{i,j,k,l}W_{i,j,k}\left(\mathbf{x}\right)\cdot\dot{\mathbf{x}}_{s,l+1/2}-\phi_{i,j,k,l}W_{i,j,k}\left(\mathbf{x}\right)\right)\mathrm{d}^3\mathbf{x}\ . \tag{51}$$

Because Eq. (49) dose not depend on $\mathbf{A}_{i,j,k,l+1}$ and $\phi_{i,j,k,l+1}$ according to Eqs. (50) and (51), $\mathbf{x}_{s,l+1}$ can be explicitly expressed in terms of quantities before the $(l+1)$-th time-step, such as $\mathbf{A}_{i,j,k,l-1}$, $\mathbf{A}_{i,j,k,l}$, $\phi_{i,j,k,l-1}$, $\phi_{i,j,k,l}$, $\mathbf{x}_{s,l-1}$, and $\mathbf{x}_{s,l}$. This provides an explicit particle pusher. Thus, the variational multi-symplectic PIC algorithm with smoothing function for the Vlasov-Maxwell system have been constructed.

In principle, the choice of electromagnetic gauge does not change the physics. However, different gauges do result in different computational complexity. We can choose the temporal gauge, $\phi=0$, to simplify the symplectic algorithm. In this gauge

$$\mathbf{E}=-\dot{\mathbf{A}}\ , \tag{52}$$

$$\mathbf{B}=\nabla\times\mathbf{A}\ , \tag{53}$$

and only electric current density and potential vector on grids are needed.

The symplectic PIC iteration is depicted in Fig. 1. We start from the quantities in the first box in the upper left corner. The position of the s-th marker $\mathbf{x}_{s,l+2}$ can be updated according to Eq. (49),

$$\mathbf{x}_{s',l+2}=2\mathbf{x}_{s',l+1}-\mathbf{x}_{s',l}+\frac{\Delta t^2}{m_{s'}}\frac{\partial}{\partial \mathbf{x}_{s',l+1}}\left[\tilde{L}_i\left(l,l+1\right)+\tilde{L}_i\left(l+1,l+2\right)\right]\ , \tag{54}$$

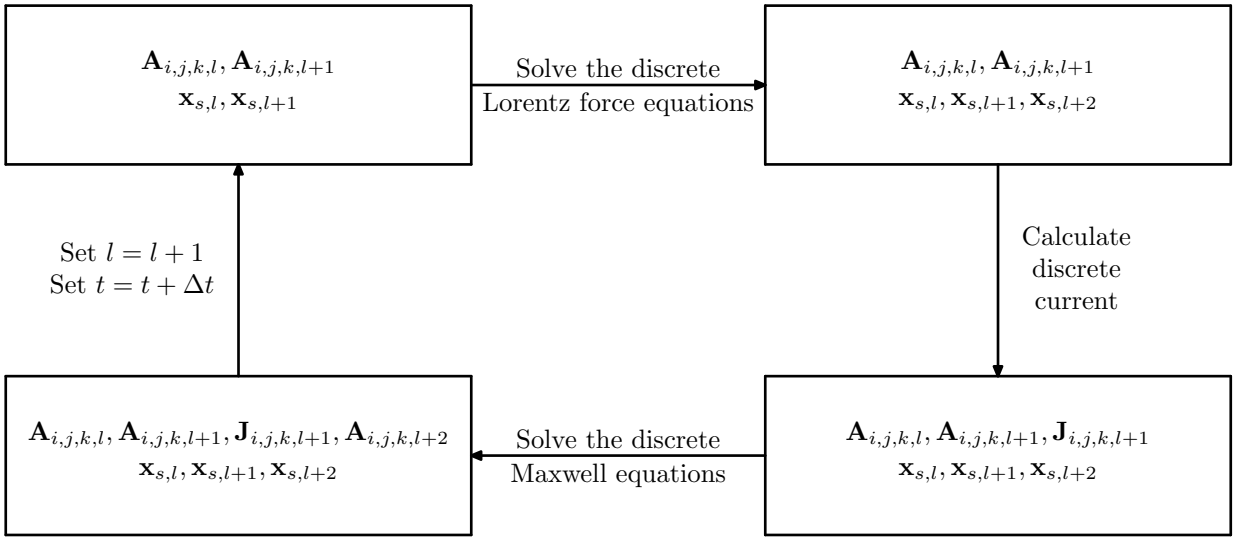

FIG. 1. A complete PIC iteration for the variational multi-symplectic algorithm with smoothing functions. The temporal gauge is adopted.

where

$$\tilde{L}_i\left(l, l+1\right) = \iiint_{\Omega} \sum_{i,j,k,s} q_s S(\mathbf{x}_{s,l} - \mathbf{x}, a) \left(W_{i,j,k}\left(\mathbf{x}\right) \mathbf{A}_{i,j,k,l} \cdot \frac{\mathbf{x}_{s,l+1} - \mathbf{x}_{s,l}}{\Delta t} \right) \mathrm{d}\mathbf{x} \ .$$

Even though in Eq. (54) $\tilde{L}_i(l+1, l+2)$ depends on $\mathbf{x}_{s,l+2}$ for all s, after the derivative with respect to $\mathbf{x}_{s',l+1}$, only the terms containing $\mathbf{x}_{s',l+1}$ are left. The result is

$$\begin{aligned} \frac{\partial}{\partial \mathbf{x}_{s',l+1}} \tilde{L}_i(l+1,l+2) = \frac{\partial}{\partial \mathbf{x}_{s',l+1}} \iiint_{\Omega} \mathrm{d}\mathbf{x} \\ \sum_{i,j,k} q'_s S(\mathbf{x}_{s',l+1} - \mathbf{x}, a) \left(W_{i,j,k}\left(\mathbf{x}\right) \mathbf{A}_{i,j,k,l+1} \cdot \frac{\mathbf{x}_{s',l+2} - \mathbf{x}_{s',l+1}}{\Delta t} \right) \ . \end{aligned} \tag{55}$$

Equation (54) gives three linear equations for the three components of $\mathbf{x}_{s',l+2}$. Thus, $\mathbf{x}_{s',l+2}$ can be solved for analytically to give an explicit relation between quantities at the l-th and $(l+1)$-th time-steps. Though this is a tedious task, symbolic algebra tools, such as the $MAXIMA$, can be used to carry out the algebraic calculation easily.

The current density $\mathbf{J}_{i,j,k,l+1}$ can be calculated from the quantities in the second upper right box in Fig. 1 using Eq. (45),

$$\mathbf{J}_{i,j,k,l+1} = \sum_s \iiint q_s S(\mathbf{x} - \mathbf{x}_{s,l+1}, a) W_{i,j,k}(\mathbf{x}) \frac{\mathbf{x}_{s,l+2} - \mathbf{x}_{s,l+1}}{\Delta t} \mathrm{d}\mathbf{x} \ . \tag{56}$$

Similarly, the potential vector $\mathbf{A}_{i,j,k,l+2}$ can be solved for the quantities in the third lower right box using Eq. (47),

$$\frac{\partial}{\partial \mathbf{A}_{i,j,k,l+1}}\left(\tilde{L}_f\left(l,l+1\right)+\tilde{L}_f\left(l+1,l+2\right)\right)+\mathbf{J}_{i,j,k,l+1}=0\ , \tag{57}$$

where

$$\begin{aligned}\tilde{L}_f\left(l,l+1\right)=&\frac{\epsilon_0}{2}\iiint_\Omega \mathrm{d}^3\mathbf{x}\left(\sum_{i,j,k}\dot{\mathbf{A}}_{i,j,k,l+1/2}W_{i,j,k}\left(\mathbf{x}\right)+\sum_{i,j,k}\phi_{i,j,k,l+1/2}\nabla W_{i,j,k}\left(\mathbf{x}\right)\right)^2\\&-\frac{1}{2\mu_0}\iiint_\Omega \mathrm{d}^3\mathbf{x}\left(\sum_{i,j,k}\nabla\times\mathbf{A}_{i,j,k,l+1/2}W_{i,j,k}\left(\mathbf{x}\right)\right)^2\ .\end{aligned}$$

In Eq. (57), $\tilde{L}_f\left(l,l+1\right)$ and $\tilde{L}_f\left(l+1,l+2\right)$ are both quadratic forms of $\mathbf{A}_{i,j,k,l}$, $\mathbf{A}_{i,j,k,l+1}$ and $\mathbf{A}_{i,j,k,l+2}$. Equation (57) is actually a matrix equation for $\mathbf{A}_{i,j,k,l+2}$ which contains $3\times N_x\times N_y\times N_z$ linear equations. Because $W_{i,j,k}(\mathbf{x})$ is locally non-zero adjacent to $\mathbf{x}_{i,j,k}$, Eq. (57) is a sparse matrix equation and can be solved using biconjugate gradient method. These procedures constitute one iteration step, which advances all the quantities to the next time-step.

The initial conditions for potentials $\mathbf{A}_{i,j,k,0}$ and $\mathbf{A}_{i,j,k,1}$ can be obtained according to the initial electromagnetic field and Eqs. (52) and (53). Moreover, $\mathbf{x}_{s,0}$ and $\mathbf{x}_{s,1}$ can be determined from the initial distribution of particles. In Sec. III, we will apply the variational multi-symplectic PIC algorithm constructed in this section. The advantage of combining symplectic algorithm with smoothing functions will be numerically verified.

III. NUMERICAL EXAMPLES

To verify the correctness and effectiveness of our variational symplectic algorithm with smoothing function, we have carried out numerical studies for typical problems in plasma physics. In these cases, we choose the interpolation function for fields $W(\mathbf{x})$ to be

$$W(\mathbf{x})=\begin{cases}(1-|x|/h)(1-|y|/h)(1-|z|/h)\ , & |x|,|y|,|z|<h\ ,\\ 0\ , & \text{otherwise}\ .\end{cases} \tag{58}$$

The smoothing function in 3D configuration space can be factorized into three 1D smoothing functions as

$$S(\mathbf{x};a)=S_1(x;a)S_1(y;a)S_1(z;a)\ , \tag{59}$$

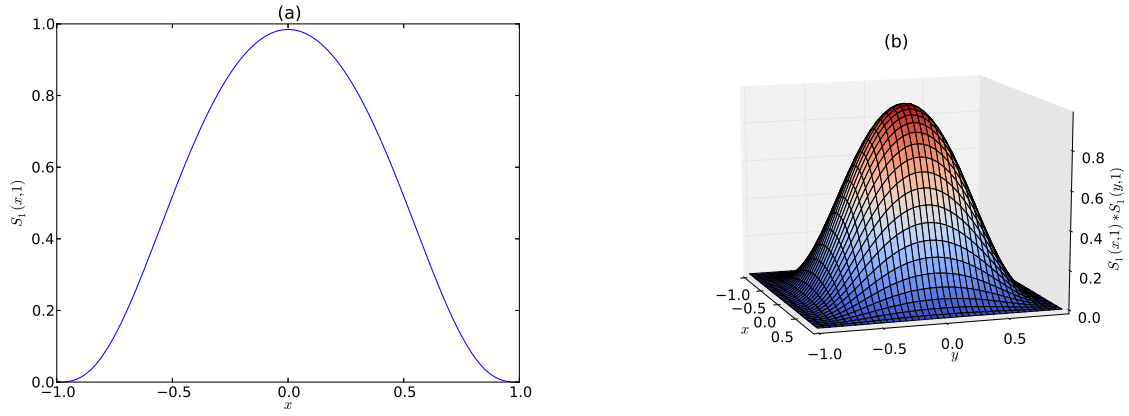

FIG. 2. 1D smoothing function $S_1(x,1)$ (a) and and 2D smoothing function $S_1(x,1)S_1(y,1)$ (b).

where the smoothing function in 1D configuration space is

$$S_1(x;a) = \alpha_1 \begin{cases} \left(1 - x^2/a^2\right)^3 \left(1 + x^2/a^2\right) \ , & |x| \le a \ , \\ 0 \ , & |x| > a \ . \end{cases} \tag{60}$$

The normalization coefficient of the 1D smoothing function is

$$\alpha_1 = \frac{63}{64}\frac{1}{a} \ . \tag{61}$$

The smoothing function is bell-shaped, which is different from Lucy's choice [20] in Eq. (16). The corresponding 1D and 2D smoothing functions are visualized in Fig. 2.

Firstly, we consider electromagnetic fluctuation in an unmagnetized plasma in equilibrium. When there is no external perturbation, the physical electromagnetic fluctuation should be very small over spatial scales much larger than the Debye length. However, the number of sampling points is much less than that of real particles, and the nonuniformity of coarse sampling in space results in severe numerical noises. To investigate the reduction of numerical noises by smoothing functions, we compare the bell-shaped smoothing function defined in Eq. (59) and the δ-function. The simulation is carried out in an $18 \times 18 \times 18$ computation domain with grid size $\Delta l = 2.4 \times 10^{-5}$m in 3D configuration space. Electrons are uniformly distributed in the configuration space and is Maxwellian in the velocity space. Ions offer a static, uniform, and positively charged background. The plasma parameters are given as follows. Thermal velocity of electrons is chosen to be 0.06c, number density of electrons is $9 \times 10^{20}\mathrm{m}^{-3}$, and the Debye length of plasma is 7.52×10^{-6}m. The time-step is set to be

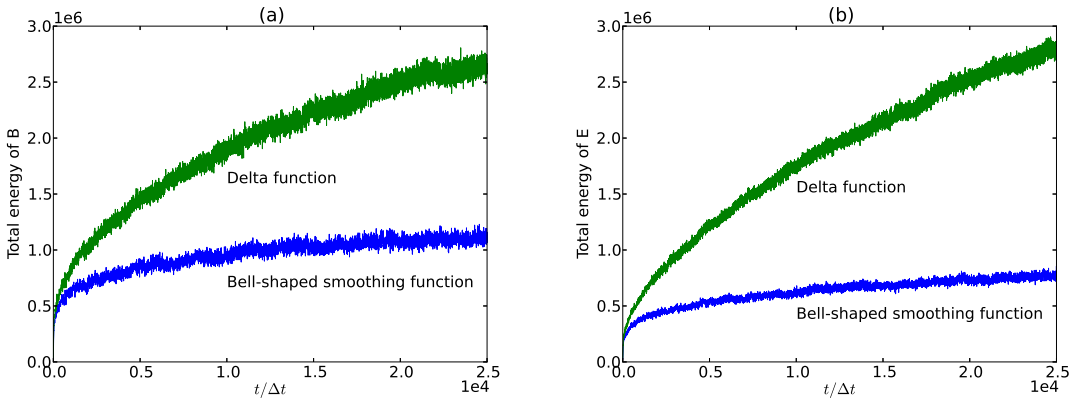

FIG. 3. Magnetic energy (a) and electric energy (b) of noise field in simulations with different smoothing functions. The simulation results with bell-shaped smoothing function are plotted in blue curves, and the simulation results with the δ-function are plotted in green curves. The reduction of noise by the smoothing function is evident. The characteristic length of shape function is $a = 0.5\Delta l$ and there are 100 markers per cell in both cases.

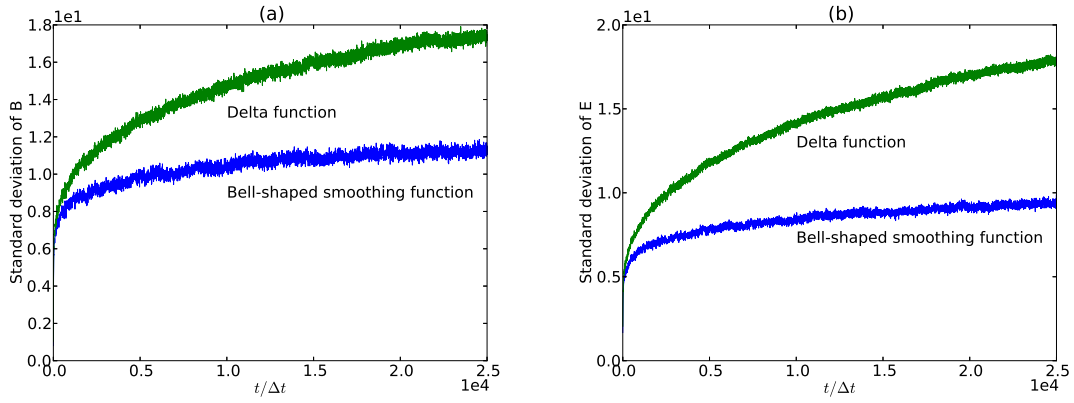

FIG. 4. Standard deviation in spatial distribution of the magnetic field (a) and the electric field (b) of the noise field in simulations with different smoothing functions. The simulation results with bell-shaped smoothing function are plotted in blue curves, and the simulation results with the δ-function are plotted in green curves. The simulation parameters are the same as in Fig. 3.

$\Delta t = 4 \times 10^{-14}$s $\approx 0.068/\omega_{pe}$. Meanwhile, the following periodic boundary conditions are

adopted,

$$\mathbf{A}_{N_x+1,j,k} = \mathbf{A}_{1,j,k} \ ,$$
$$\phi_{N_x+1,j,k} = \phi_{1,j,k} \ ,$$
$$\mathbf{A}_{i,N_y+1,k} = \mathbf{A}_{i,1,k} \ ,$$
$$\phi_{i,N_y+1,k} = \phi_{i,1,k} \ ,$$
$$\mathbf{A}_{i,j,N_z+1} = \mathbf{A}_{i,j,1} \ ,$$
$$\phi_{i,j,N_z+1} = \phi_{i,j,1} \ .$$

Simulation results depict the growth of numerical noises of electromagnetic fields from null initial values in Fig. 3 and 4. Figure 3 shows the total magnetic energy and the total electric energy of the fluctuation field. Plotted in Fig. 4 is the spatial standard deviation of the magnetic field and the electric field. The numerical noise is evidently reduced and rapidly saturated at a low level with the application of the bell-shaped smoothing function, in contrast to the δ-function case, where the noise level keeps growing. In this comparison, we have chosen the smoothing function parameter to be $a = 0.5\Delta l$. If we choose a larger a, the reduction of noise level will be more prominent at the expense of more computation time.

In the next example, we simulate a harmonic standing wave in the above computation domain to test the convergency and effectiveness of the algorithm. The grid size Δl is reset to 4.4×10^{-5}m. A harmonic standing wave is initialized in the unmagnetized plasma with periodic boundary conditions. After the evolution of 1.2×10^4 time-steps, it can be observed that important differences appear between the simulations with different smoothing functions, see Fig. 5. The standing wave structure is well maintained in the simulation with bell-shaped smoothing function. But for the simulation using the δ-function as the smoothing function, numerical noise is so large that it almost outgrows the physical perturbation.

Finally, we investigate the electromagnetic fluctuation in a magnetized plasma to verify the long-term conservation properties of this algorithm. As a symplectic algorithm, this PIC method has good long-term conservation properties. The numerical error of all conserved quantities should be bounded by a small value and not increase with time. The background magnetic field is selected to be $B_0 = 1T$. The time-step is $\Delta t = T/8.1$, where T is the gyro-period of electrons. At $t = 0$, an arbitrary perturbation which does vary along the

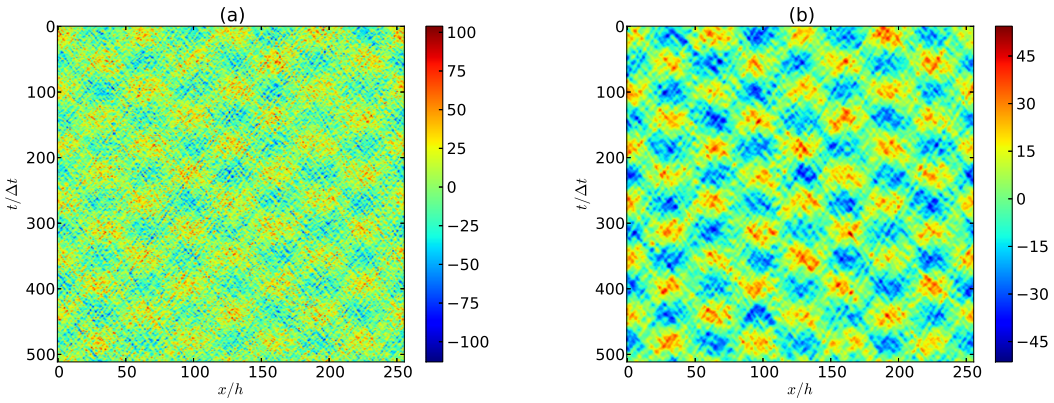

FIG. 5. After evolution of 1.2×10^4 time-steps, the simulation results of a harmonic standing wave in an unmagnetized plasma are different with the application of different smoothing functions. The standing wave structure is well-maintained in the simulation with the bell-shaped smoothing function (b) and is dominated by the noise with the δ-function (a). The characteristic length of the bell-shaped smoothing function is chosen to be $a = 0.5\Delta l$.

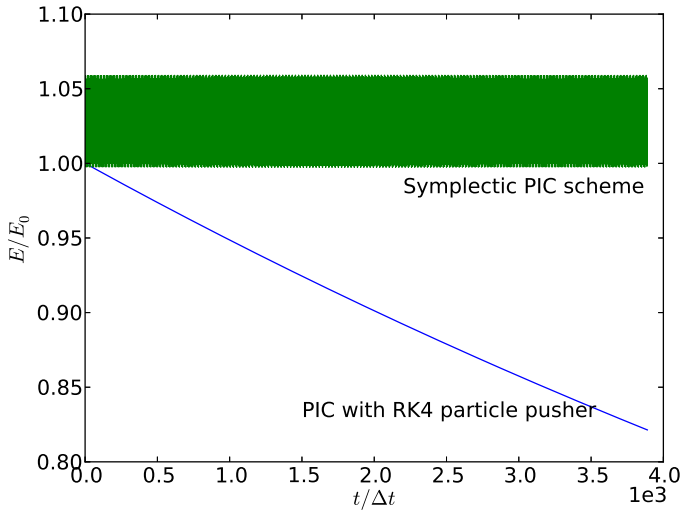

FIG. 6. The evolution of total energies of a magnetized plasma simulated with different algorithms. The blue curve is the result using the non-symplectic method, while the green curve is the result using the variational multi-symplectic algorithm. It's obvious that the symplectic algorithm bounds the long-term energy error.

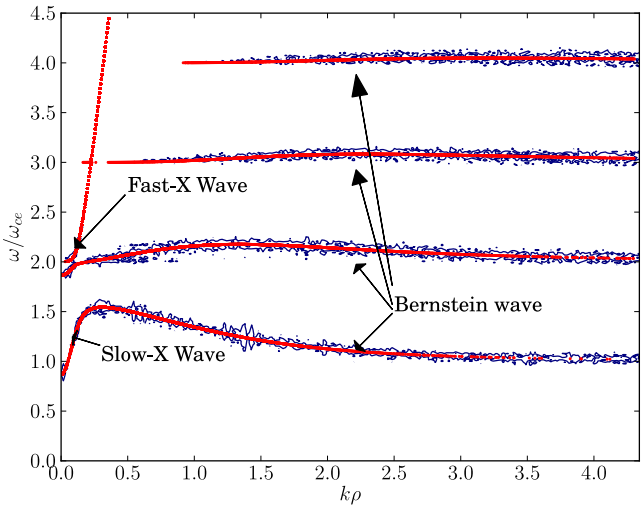

FIG. 7. The space-time spectrum of high frequency waves in magnetized plasmas simulated by the variational multi-symplectic PIC algorithm with smoothing function. The numerial dispersion relations (the blue contours) agree with analytical results (the red curves).

magnetic field is launched. The system is then evolved using this symplectic algorithm. A non-symplectic algorithm, which uses the forth-order Runge-Kutta method (RK4) to push particles and a finite difference method to solve for fields, is also applied for comparison. The total energy of the plasma is recorded at every time-step, see Fig. 6. The total energy of the system decays for the non-symplectic algorithm, while it is bounded within a small value ΔE_M for the symplectic algorithm. The maximum energy error ΔE_M of the symplectic integrator is approximately proportional to the size of time-step Δt in this case because the particle pusher used here is a first-order algorithm. The space-time spectrum of the electromagnetic fluctuation simulated using the symplectic algorithm is plotted in Fig. 7. The dispersion curves of X waves in low wave-number region and that of electron Bernstein waves in high wave-number region agree with the analytical results very well.

IV. SUMMARY AND DISCUSSION

In this paper, we have introduced a method to construct a variational multi-symplectic algorithm with smoothing function for Vlasov-Maxwell equations. This algorithm can effectively reduce the numerical noises caused by coarse sampling of particles in full-f PIC

simulations. At the same time, it also has the good conservation properties and long-term numerical stability associated with symplectic algorithms. Simulation results with different smoothing functions were carried out for comparison. The reduction of numerical noise by smoothing function and good conservation properties were verified by numerical examples. The variational multi-symplectic PIC algorithm can be extended to more general cases. For example, the electromagnetic field can be discretized on other types of meshes, such as tetrahedron mesh. When discretizing the Lagrangian density, we can use a method different from the mid-point method to construct an explicit solver for electromagnetic fields. Other techniques, such as the δf method, can also be used to reduce numerical noises in PIC simulation. Although the δf method is widely adopted in non-symplectic algorithms, the construction of a symplectic δf PIC method is still an open question. This topic will be investigated in our future study.

---

[1] E. Hairer, C. Lubich, and G. Wanner, *Geometric numerical integration: structure-preserving algorithms for ordinary differential equations*, Vol. 31 (Springer, 2006).

[2] R. D. Ruth, IEEE Trans. Nucl. Sci **30**, 2669 (1983).

[3] K. Feng, Journal of Computational Mathematics **4**, 279 (1986).

[4] K. Feng and M. Qin, *The symplectic methods for the computation of Hamiltonian equations* (Springer, 1987) pp. 1–37.

[5] R. De Vogelaére, Department of Mathematics, University of Notre Dame, Report **4** (1956).

[6] A. P. Veselov, Funct. Anal. Appl. **22**, 83 (1988).

[7] A. Lew, J. E. Marsden, M. Ortiz, and M. West, Arch. Ration. Mesh. Anal. **167**, 85 (2003).

[8] D. Pavlov, P. Mullen, Y. Tong, E. Kanso, J. Marsden, and M. Desbrun, Physica D: Nonlinear Phenomena **240**, 443 (2011).

[9] E. Gawlik, P. Mullen, D. Pavlov, J. Marsden, and M. Desbrun, Physica D: Nonlinear Phenomena **240**, 1724 (2011).

[10] J. Marsden, M. West, *et al.*, Acta Numerica **10**, 514 (2001).

[11] H. Qin and X. Guan, Phys. Rev. Lett. **100**, 035006 (2008).

[12] H. Qin, X. Guan, and W. M. Tang, Phys. Plasmas **16**, 042510 (2009).

[13] M. Desbrun, A. N. Hirani, M. Leok, and J. E. Mardsen, e-print arXiv:-math/0508341 (2005).

[14] J. Squire, H. Qin, and W. Tang, Physics of Plasmas **19**, 084501 (2012).

[15] C. K. Birdsall and A. B. Langdon, *Plasma Physics via Computer Simulation* (McGraw-Hill, Inc., 1985).

[16] G. Liu and M. Liu, *Smoothed particle hydrodynamics: a meshfree particle method* (World Scientific Publishing Company Incorporated, 2003).

[17] J. Marsden, G. Patrick, and S. Shkoller, Communications in Mathematical Physics **199**, 351 (1998).

[18] H. Qin, R. H. Cohen, W. M. Nevins, and X. Q. Xu, Phys. Plasmas **14**, 056110 (2007).

[19] F. E. Low, Proc. R. Soc. Lond. A **248**, 282 (1958).

[20] L. Lucy, The astronomical journal **82**, 1013 (1977).

[21] J. R. Shewchuk, *An introduction to the conjugate gradient method without the agonizing pain* (Carnegie Mellon University, Pittsburgh, PA, 1994).

The Princeton Plasma Physics Laboratory is operated
by Princeton University under contract
with the U.S. Department of Energy.

Information Services
Princeton Plasma Physics Laboratory
P.O. Box 451
Princeton, NJ 08543

Phone: 609-243-2245
Fax: 609-243-2751
e-mail: pppl_info@pppl.gov
Internet Address: http://www.pppl.gov